Monte Carlo study of the three-dimensional Coulomb frustrated Ising ferromagnet

M. Grousson,[1] G. Tarjus,[1] and P. Viot[1,2]
[1]*Laboratoire de Physique Théorique des Liquides, Université Pierre et Marie Curie, 4 Place Jussieu, 75252 Paris Cedex 05, France*
[2]*Laboratoire de Physique Théorique, Bâtiment 210, Université Paris-Sud, 91405 Orsay Cedex, France*
(Received 17 April 2001; published 20 August 2001)

We have investigated, by Monte Carlo simulation, the phase diagram of a three-dimensional Ising model with nearest-neighbor ferromagnetic interactions and small, but long-range (Coulombic) antiferromagnetic interactions. We have developed an efficient cluster algorithm and used different lattice sizes and geometries, which allows us to obtain the main characteristics of the temperature-frustration phase diagram. Our finite-size scaling analysis confirms that the melting of the lamellar phases into the paramagnetic phase is driven first order by the fluctuations. Transitions between ordered phases with different modulation patterns are observed in some regions of the diagram, in agreement with a recent mean-field analysis.

DOI: 10.1103/PhysRevE.64.036109 PACS number(s): 05.50.+q, 05.70.Fh, 64.60.Cn

I. INTRODUCTION

Models with a competition between a short-range ordering interaction and a long-range frustrating interaction are relevant to describe a large number of experimental systems in soft-matter physics (diblock copolymer melts [1], cross-linked polymer mixtures [2] and interpenetrating networks [3], oil-water surfactant mixtures [4–6]) and in magnetism (ultrathin magnetic films [7–9]). These are also invoked to explain glass formation in quite different situations such as doped Mott insulators [10–12] and supercooled liquids [13,14]. Some generic features shown by these models are the existence of mesophases characterized by modulated spatial patterns and the importance of the fluctuations that strongly influence the physics at and above the transition to these various phases.

A simple version of a system with such a uniform frustration consists of a Coulomb frustrated Ising ferromagnet, in which Ising spins placed on a three-dimensional cubic lattice, interact via both nearest-neighbor ferromagnetic couplings and long-range Coulombic antiferromagnetic couplings. The mean-field theory [15] predicts a complex temperature-frustration phase diagram in which the low-temperature region displays infinite sequences of commensurate and incommensurate modulated phases and is separated from the high-temperature paramagnetic region by a line of second-order phase transitions. However, both an analytical work based on the self-consistent Hartree approximation [16] and a first Monte Carlo study [17] indicate that the fluctuations drive the transition from second to first order. At least in the region around the transition, the mean-field phase diagram is thus dubious.

The purpose of this paper is to thoroughly investigate, by Monte Carlo simulations, the main characteristics of the phase diagram of the Coulomb frustrated Ising model. Compared to other systems, this model poses several serious difficulties to computer simulations: one stems from the long-range nature of the frustrating interaction and the other concerns finite-size studies of phases with modulated order. After briefly presenting the model and reviewing the results of previous work (Sec. II), we discuss in Sec. III the methodological aspects of our Monte Carlo simulations. We have used two different algorithms: a cluster algorithm for small frustration and a parallel tempering method for large frustration. The results, concerning the nature of the transition between the paramagnetic and the modulated phases, are presented in Sec. IV. A careful finite-size scaling analysis confirms the first-order character of this transition. We also give, in this section, a selected study of transitions between different modulated phases.

II. THE COULOMB FRUSTRATED ISING FERROMAGNET

A. The model

The Hamiltonian of the model is

$$H = -J\sum_{\langle i,j\rangle} S_i S_j + \frac{Q}{2}\sum_{i\neq j} v(\mathbf{r}_{ij}) S_i S_j , \tag{1}$$

where J and Q are both positive and denote the strength of the ferromagnetic and the antiferromagnetic interaction, respectively; $S_i = \pm 1$, is the Ising spin variable, and the bracket $\langle i,j\rangle$ means that the summation is restricted to distinct pairs of nearest neighbors; $\mathbf{r}_{ij}$ is the distance between the sites i and j on a three-dimensional cubic lattice, and $v(\mathbf{r})$ represents a Coulomb-like interaction term such that $v(\mathbf{r}) \sim 1/|\mathbf{r}|$ when $|\mathbf{r}| \to \infty$.

Because of the Coulomb interaction, the existence of the thermodynamic limit requires that the total magnetization of the system be zero. As a consequence, the ferromagnetic order is forbidden at all temperatures and for any nonzero value of the frustration parameter Q/J. In three dimensions, one expects this system to have an order-disorder transition at finite temperature, but contrary to the case of the unfrustrated system, the low-temperature ordered region exhibits a complex frustration-temperature phase diagram with a variety of modulated phases. We first summarize the exact results obtained for the ground states and the results of the mean-field theory [15], which both have guided the Monte Carlo simulations.

B. Ground states

At zero temperature, the phase diagram can be calculated exactly. It was done numerically for $v(\mathbf{r})$ equal to the true Coulombic interaction $(1/\mathbf{r})$ and analytically for $v(\mathbf{r})$ expressed in terms of the lattice Green function [15]. For small values of the frustration parameter, the ground state consists of lamellar phases in which lamellae of width m, made up by parallel planes of ferromagnetically aligned spins, form a periodic structure of length $2m$ along the orthogonal direction. When the frustration increases, the period of the lamellar phases decreases until one reaches $m=1$. Each lamellar phase is the ground state for a finite interval of the frustration parameter Q/J. When this latter goes to zero, the width of lamellae diverges as $(Q/J)^{-1/3}$ and the range of stability of the successive lamellar phases shrinks to zero as $(Q/J)^{4/3}$. For $Q/J<1$, the ground states obtained by the numerical calculation for the true Coulombic potential and those obtained by the analytical calculation for the inverse lattice Laplacian are almost identical.

For larger values of the frustration parameter Q/J, the system loses the translational invariance in a second direction and the ground states then consist of tubular phases. Eventually, the translational invariance is lost in the third direction and the ground states are orthorhombic phases. In the limit of large frustrations, the ground state is a Néel antiferromagnetic phase [15]. Even if the sequence of ground states is the same for the true Coulombic potential and for the inverse lattice Laplacian potential, the sequence of frustration parameters to which these ground states are associated is more and more different when Q/J increases. In the following, we focus on the region of small or moderate frustration parameters $(Q/J\leqslant 1)$.

C. Frustration-temperature phase diagram

At finite temperature, the phase diagram can no longer be obtained exactly. We summarize here the results obtained within different approximations. A detailed analysis has been performed within the mean-field approximation [15]. For each frustration parameter Q/J, there is a continuous transition at finite temperature between the disordered phase and modulated phases. The wave vector that characterizes the modulation at the transition varies continuously with the frustration parameter; as a result, a succession of incommensurate modulated phases is predicted along the transition line. As shown in Fig. 1, the phase diagram is divided into two main regions: above the transition line (full line), the system is disordered (paramagnetic), whereas an infinite number of modulated phases exists at low temperatures (only a few of them are displayed in Fig. 1). When Q/J goes to zero, the line of critical points goes continuously, but nonanalytically toward T_c^0, the critical temperature of the unfrustrated Ising model. To describe the low-temperature region, it is convenient to use the short-hand notation introduced by Fisher and Selke [18] for characterizing modulated phases: $\langle m_1^{n_1} m_2^{n_2}, \ldots, m_p^{n_p}\rangle$ designates a modulated phase formed by the periodic repetition of a fundamental pattern consisting of a succession of n_1 lamellae of width m_1, followed by n_2 lamellae of width m_2, and so on, where the m_i's and the n_i's are integers and where two successive lamellae are composed of spins of opposite sign. From the zero temperature axis springs an infinite number of quasivertical lines that separate the various simple lamellar phases $\langle m\rangle$. At finite (nonzero) temperatures, these lines split into branches separating phases with more complex modulations, each branch splitting itself at higher temperature into new branches, etc., according to ''structure combination branching processes'' [19]. Close to the transition line, one expects incommensurate phases. By using the soliton approach developed by Bak and co-workers [20,21], an approach that focuses on the behavior of the domain walls that separate commensurate regions, one can study the melting of commensurate phases into incommensurate phases; the resulting lines are shown as the dotted and dashed curves in Fig. 1.

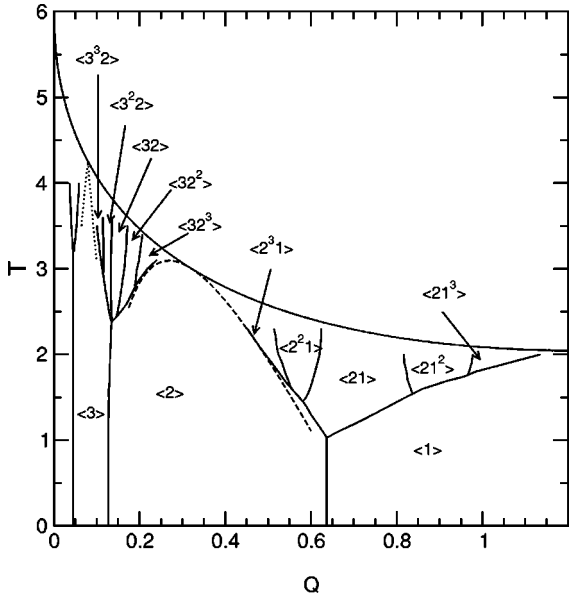

FIG. 1. Temperature-frustration mean-field phase diagram. There is an infinite sequence of flowers of complex modulated phases appearing at finite temperatures in the range of the frustration parameter for which the ground states are simple lamellar phases. The units are chosen such that $k_B=J=1$.

In addition to the mean-field description, the mean-spherical version of this model, in which spins are taken to be real numbers with the global constraint that their mean-square value is equal to one, has also been studied [22]. In three dimensions, the transition between disordered and modulated phases is also predicted to be continuous, albeit with a feature coined ''avoided critical behavior'' [22]; for vanishing frustration, the transition temperature goes to a value that is much below the temperature T_c^0 of the unfrustrated model. Nussinov *et al.* [23] have subsequently shown that this behavior remains for spin variables with $O(n)$ symmetry whenever $n>2$. For $n=1$ (Ising spins), one expects the Coulomb frustrated model to be in the Brazovskii class of Hamiltonians [16] and consequently, as predicted from a self-consistent Hartree approximation, to display a first-order transition between modulated and disordered phases. Since the mean-field approximation predicts a continuous transi-

tion (see above), the change of order of the transition is induced by the fluctuations.

III. SIMULATIONS

A. Introduction

The Coulombic interaction is the source of several difficulties and limitations for computer simulations that we now review.

(i) To properly account for the long-range nature of the interactions in systems with periodic boundary conditions, the minimum image convention used in models with short-range interactions cannot be used, and a complete calculation of the site-site interaction terms requires considering all the images of the simulation basic cell, a procedure that is realized by using Ewald sums [24]. For a lattice system, the site-site pair interaction terms are calculated once for all at the beginning of the run and are stored in an array for the entire run. Therefore, a large number of reciprocal vectors can be included in the Ewald sum, which ensures a very good accuracy for the calculation of the Coulomb potential.

(ii) For a single spin flip, the energy update involving Coulombic terms is performed by summing over all lattice sites. Therefore, for a lattice with a linear size L and with a constant Monte Carlo swap per spin, the computer time is proportional to L^6 for a system with Coulombic interactions whereas it goes only as L^3 for a system with short-range interactions. For a given computer time, the maximum linear size that one can consider for the Coulomb frustrated model systems is then roughly the square root of the linear size of its counterpart without frustration. This strongly limits the largest system size that can be studied with the present computer capabilities (typically $L \simeq 20$).

(iii) The mean-field analysis summarized above has revealed that upon decreasing the temperature at a fixed value of the frustration parameter Q/J, the system undergoes a sequence of phase transitions involving different modulations before reaching the ground state. This complex phase diagram corresponds, of course, to a system in the thermodynamic limit. In a Monte Carlo study, one must perform a finite-size analysis in order to extrapolate to the limit of an infinite system. For simple models in which only a finite number of phases are present, one has to study a finite number of transition lines; increasing the size of the system progressively moves these lines toward their location in the thermodynamic limit. In the present model, a small temperature range may include a large number of modulated phases that may or may not be observed in a finite system depending on the commensurability between the period of the modulation and the linear size of the system. Upon increasing the latter, not only do the phase boundaries move (as in a standard model), but new phases with more complex modulation patterns may appear as well. This feature, akin to a process of degeneracy lifting, makes the finite-size analysis much more difficult.

(iv) To ensure that the proper ground state is obtained, the size of the lattice must be compatible with the period of the expected lamellar phase. For instance, for a ground state corresponding to an $\langle m \rangle$ phase, a system of size $2pm$ with $p \geqslant 1$ in at least one direction must be used, otherwise, the system misses the proper phase transition, and the energy in the low-temperature region is much higher than that obtained with commensurate lattice sizes. This limits the range of frustration parameters that can be studied.

A first Monte Carlo study [17] was performed by using a Metropolis algorithm with the constraint of zero total magnetization. The phase boundary between the paramagnetic phase and the modulated phases was located. The double peak structure of the energy histograms close to the transition region, and the occurrence of a hysteresis loop between heating and cooling, runs strongly, suggesting that the transition is first order. The purpose of the present work is to complete this first study by a more exhaustive investigation of the phase diagram and a finite-size scaling analysis. In order to achieve this, more efficient algorithms have been developed. In all simulations, the true Coulomb potential $v(r) = 1/|r|$ is used.

B. Cluster algorithm

For continuous and weak first-order transitions, cluster algorithms improve the convergence of Monte Carlo runs close to the transition [25]. Let us briefly review the available methods; the standard cluster algorithms (Swendsen-Wang [26] and Wolff [27]) take advantage of a local symmetry, like the up-down spin symmetry, but they cannot be used for systems that have the constraint of zero total magnetization. For Hamiltonians with algebraic interactions, an efficient full cluster method has been developed [28–30], that generalizes the Swendsen-Wang (or Wolff) algorithm to long-range interactions. This method, as with the previous ones, requires the existence of a local symmetry and cannot be straightforwardly applied to Coulombic systems. (Recall that in the present model this constraint stems from the existence of the thermodynamic limit.) Recently, Dress and Krauth [31] have introduced a cluster algorithm that makes use of the geometrical symmetries of the system. These symmetries are conserved even in the presence of the constraint of zero total magnetization. Dress and Krauth first studied a hard-sphere system. Herringa and Blöte [32] subsequently implemented this algorithm for a lattice gas (or correspondingly an Ising spin system) with short-range interactions. The procedure is the following: two thermal clusters of opposite signs are simultaneously grown by randomly choosing a seed site and its symmetric counterpart obtained through a geometrical symmetry (translation, rotation, inversion, . . .) of the Hamiltonian; the clusters are built by adding neighboring spins of the same orientation with the probability $p = [1 - \exp(-4\beta J)]$. It can be shown that, provided the symmetry group allows for particles to reach any site of the system, the algorithm satisfies ergodicity, and the detailed balance is given by

$$T^{\beta}_{i\to j} A^{\beta}_{i\to j} P^{\beta}_{i} = T^{\beta}_{j\to i} A^{\beta}_{j\to i} P^{\beta}_{j}, \tag{2}$$

where $T^{\beta}_{i\to j}$ denotes the probability of growing two clusters whose global flips transform a spin configuration i into j, $A^{\beta}_{i\to j}$ is the acceptance ratio for this change of configurations,

and P_i^β is the Boltzmann distribution. With the two clusters built with the bond probability $p=[1-\exp(-4\beta J)]$, one can easily show that [32]

$$\frac{T_{i\to j}^\beta}{T_{j\to i}^\beta}=\frac{P_j^\beta}{P_i^\beta}. \tag{3}$$

As can be checked by substituting Eq. (3) in Eq. (2), one can then choose $A_{i\to j}^\beta=1$, i.e., the flip of a cluster is always accepted [33].

For systems whose Hamiltonians can be divided into two parts, a reference Hamiltonian H_0 with short-ranged interactions and a Hamiltonian H_1 with long-ranged interactions, we propose the following hybrid cluster algorithm. The clusters are built with bonds corresponding to the reference Hamiltonian, but instead of accepting all the Ising clusters that are formed, the detailed balance is now expressed as

$$\frac{A_{i\to j}^\beta}{A_{j\to i}^\beta}=\exp(-\beta\Delta E_1^{ji}), \tag{4}$$

where ΔE_1^{ji} is the difference of energy between the jth and the ith configurations for the Hamiltonian H_1. Equation (4) is fulfilled if $A_{i\to j}^\beta$ is chosen according to a Metropolis rule: the new configuration is accepted if $\Delta E_1^{ji}<0$, otherwise a random number η is chosen between 0 and 1 from a uniform distribution and the new configuration is accepted if $\eta<\exp(-\beta\Delta E_1^{ji})$.

This algorithm remains efficient if $(\beta\Delta E_1^{ji})\simeq 0$ for most generated configurations; the rate of acceptance is then close to 1 and most generated configurations are accepted [34]. Unfortunately, for our model, the long-range antiferromagnetic interaction never satisfies the above condition, and the acceptance ratio is then very small; clusters are almost never flipped, and the procedure becomes inefficient.

In order to construct a better cluster algorithm, let us first analyze the drawback of the above method. Close to the transition temperature, the clusters, which have been built by using the reference Hamiltonian, are actually too large. Indeed they have been generated with a bond probability that is too large because it corresponds, for the reference system, to a temperature that is located below its critical temperature. Close to the transition temperature $T_c(Q/J)$, the typical excitations in the pure Ising model are much larger than those for the frustrated system because the existence of large domains is prevented in the latter by the frustration [recall that $T_c(Q/J)<T_c^0$]. As a consequence, the acceptance ratio becomes very small and the generated clusters are almost never flipped.

It is possible to obtain a more reasonable acceptance ratio by modifying the above procedure as follows: two thermal clusters of opposite signs are grown simultaneously by randomly choosing a seed site and its symmetric counterpart obtained through a geometrical symmetry (translation, rotation, inversion, ...) of the Hamiltonian. One then adds neighboring spins of the same orientation in each cluster with the probability $[1-\exp(-4\beta_{eff}J)]$ where $\beta_{eff}<\beta$.

The detailed balance is given by

$$T_{i\to j}^{\beta_{eff}}A_{i\to j}^{\beta_{eff}}P_i^\beta=T_{j\to i}^{\beta_{eff}}A_{j\to i}^{\beta_{eff}}P_j^\beta, \tag{5}$$

where all quantities are defined below Eq. (2). Combining Eqs. (5) and (3) (this latter being expressed from the reference Hamiltonian) one obtains

$$\frac{A_{i\to j}^{\beta_{eff}}}{A_{j\to i}^{\beta_{eff}}}=\exp[-\beta\Delta E_1^{ji}+(\beta_{eff}-\beta)\Delta E_0^{ji}], \tag{6}$$

where ΔE_0^{ji} is the energy difference between the jth and the ith configurations for the reference Hamiltonian.

Note that when $\beta_{eff}\to 0$, the cluster size goes to 1, and one recovers a two-spin Metropolis rule. For nonzero β_{eff}, the Metropolis rule for the cluster acceptance is the following: the new configuration is accepted if $\Delta E_1^{ji}+(1-\beta_{eff}/\beta)\Delta E_0^{ji}<0$, otherwise, a random number η is chosen between 0 and 1 from a uniform distribution and the new configuration is accepted if $\eta<\exp[-\beta\Delta E_1^{ji}+(\beta_{eff}-\beta)\Delta E_0^{ji}]$.

In preliminary runs, β_{eff} has been tuned to obtain the highest acceptance ratio. We have found that this latter is attained for an effective temperature slightly above the critical temperature of the unfrustrated Ising model ($T_{\text{eff}}\simeq 5$). For higher effective temperatures, the cluster size decreases very rapidly and the algorithm then reduces to a Metropolis algorithm. When $T_{\text{eff}}\simeq 5$, the system jumps from disordered states to modulated states and vice versa along the run, which suppresses the hysteresis between heating and cooling runs observed in simulations performed with a simple Metropolis algorithm [17]. Since the system is now equilibrated at each temperature, one observes a double-peak structure (in the energy histograms around the transition temperature) and it is possible to determine the value of the specific heat at the transition.

In addition to this hybrid cluster algorithm, we have also implemented a parallel tempering algorithm. First introduced by Hukusima and Nemoto [35] in the context of spin glass models, this method belongs to the class of multicanonical Monte Carlo algorithms [36] which are well adapted for the study of first-order transitions. For a small frustration parameter $Q/J<0.1$, the first-order character of the transition from disordered to modulated phases is expected to be rather weak, and the hybrid cluster algorithm has a better convergence. For $0.1<Q/J<1$, the two methods have a comparable efficiency. For $Q/J\geqslant 1$, the energy discontinuity becomes higher, and the parallel tempering method is the most efficient.

IV. RESULTS

A. Melting of the simple lamellar phases

A first series of simulations has been performed for estimating the location of the transition line that separates the paramagnetic phase from the modulated phase. The transi-

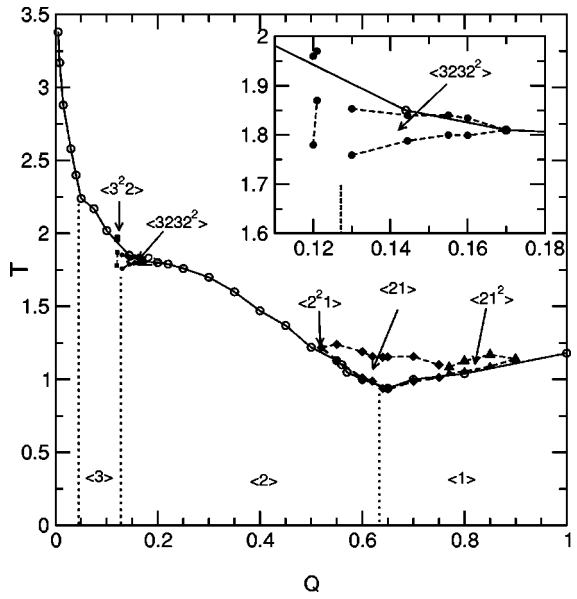

FIG. 2. Phase diagram obtained by Monte Carlo simulation. The melting line of the simple lamellar phases (full, dark curve, and open symbols) displays cusps around $Q \simeq 0.04$, $Q \simeq 0.13$, and $Q \simeq 0.65$. In these regions, intermediate modulated phases appear that correspond to mixed lamellar phases (dashed lines and filled symbols). The inset zooms in on the region between the $\langle 2 \rangle$ and $\langle 3 \rangle$ phases. The units are chosen such that $k_B = J = 1$.

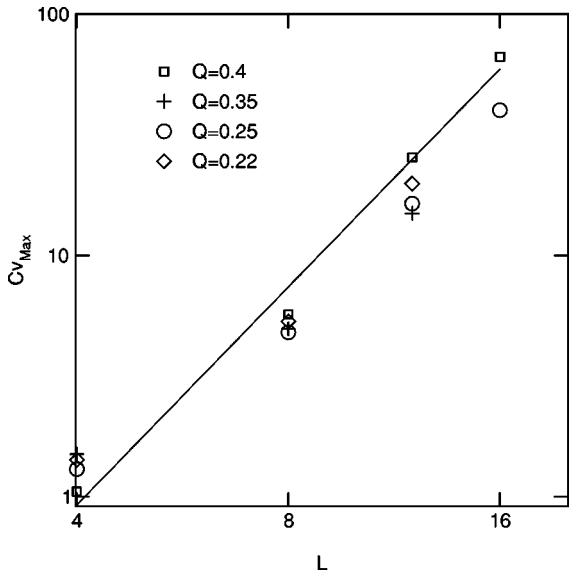

FIG. 3. Log-log plot of the maximum of the specific heat vs the linear lattice size for $Q/J = 0.2$, 0.22, 0.35, and 0.4 ($L = 4$, 8, 12, and 16). The straight line corresponds to an L^3 behavior.

tion temperature for each value of Q/J has been estimated by first monitoring the melting of the (known) ground state when increasing the temperature. The results are shown as open symbols (and full, dark line) in Fig. 2. The decrease of the transition temperature T_c with increasing frustration is more rapid than in the mean-field approximation; T_c/J drops from 4.51 for $Q = 0$, to 3.38 for $Q/J = 0.005$, and to 2.02 for $Q/J = 0.1$. For the largest frustration studied, $Q/J = 1$, $T_c/J \simeq 1.2$, one notices, however, some peculiar features of the transition line so obtained; small cusps are observed around $Q/J \simeq 0.04$, $Q/J \simeq 0.13$, and $Q/J \simeq 0.65$; this latter case even corresponds to an absolute minimum of the transition curve with $T_c/J \simeq 0.934$. These features can be understood by comparing with the mean-field phase diagram in Fig. 1. The cusplike regions precisely correspond to the location of the springing ''flowers'' of phases with complex modulations, and our study with limited system sizes misses the appearance of these modulated phases.

Before coming back to the above point in more detail, we first address the question of the order of the transition to the paramagnetic phase. To do so, we restrict the analysis to a range of frustration parameters for which the interference of mixed lamellar phases with complex modulation patterns is expected to be minimal; for Q/J between 0.2 and 0.4, one expects a direct melting of the ground state, the simple lamellar phase $\langle 2 \rangle$, into the disordered phase (see Figs. 1 and 2). For several values of Q/J (0.2, 0.22, 0.35, and 0.4), we have performed a finite-size scaling analysis of the transition by varying the linear size L of the lattice from $L = 4$ to $L = 16$. We have computed the maximum of the specific heat $C_v^{max}(L)$ and the shift of the apparent transition temperature $T_c(L)$. (Since the total magnetization is set to zero, the corresponding Binder cumulants cannot be used for this model.) For a first-order phase transition, the scaling laws for these quantities are $C_v^{max} = c_0 L^k$ and $T_c(L) = T_c(\infty) + \alpha L^{-k}$, where k is equal to d, the dimension of the system.

The maximum of the specific heat versus L is displayed on a ln-ln plot in Fig. 3. The best linear square fit gives an exponent $k = 3.00 \pm 0.21$ for $Q/J = 0.4$, which is in very good agreement with the value expected for a first-order transition. (As shown in Fig. 3, for the other values of Q/J, k is also compatible with the value of 3.) The same analysis have been performed for the shift of the apparent transition temperature, and the corresponding fits are also in good agreement with $k = d = 3$. This clearly shows that, at least in the range of frustration parameters where finite-size scaling is achievable, the transition between the paramagnetic and the modulated phases is a first-order one.

B. Transitions involving mixed lamellar phases

For temperatures below the disordered-modulated transition, the mean-field theory predicts that the system undergoes a series of transitions to various commensurate and, possibly, incommensurate phases, which gives to the phase diagram the flowerlike structure illustrated in Fig. 1. Because of the finite size of the system studied in simulations, it is not possible to observe incommensurate phases, but one can expect to detect transitions between different commensurate phases, provided that the lattice size is commensurable with the periods of the distinct modulated phases. Since the required lattice sizes are larger than the maximum size of cubic simulation cells compatible with reasonable computer time, we have used anisotropic simulation cells. The main advantage is that the computer time increases only like $l^4 L^2$, where L is the largest linear size of the lattice and l is the size in the perpendicular directions, instead of L^6 for cubic cells. Note

that, because of the anisotropy, finite-size scaling arguments cannot be applied in a simple way. To characterize the transition between different modulated phases, we have here monitored the order parameter $|M(\mathbf{k})|^2$, which is defined as

$$|M(\mathbf{k})|^2 = \langle \hat{S}(\mathbf{k}) \rangle \langle \hat{S}(-\mathbf{k}) \rangle = \frac{1}{N} \left\{ \left\langle \sum_{i=1}^{N} [S_i \cos(\mathbf{k} \cdot \mathbf{r}_i)] \right\rangle^2 + \left\langle \sum_{i=1}^{N} [S_i \sin(\mathbf{k} \cdot \mathbf{r}_i)] \right\rangle^2 \right\}, \quad (7)$$

where N is total number of spins on the lattice and the brackets denote a thermal average. For each of the three directions of the lattice, the wave-vector components are equal to $2\pi p/L$, with p going from $-L/2+1$ to $L/2$. Since the total magnetization must be zero, L has to be an even number and the $k=0$ component of the order parameter is always zero. The periodic boundary conditions imply that $|M(k=2p\pi/L)|=|M(k=-2p\pi/L)|$, where $p=1,\ldots,(L/2-1)$. After adding the last component $|M(k=\pi)|$ (corresponding to $p=L/2$) the number of independent wave vectors for each direction is then $L/2$. All components of the order parameter vanish in the paramagnetic phase, whereas one or several components are different from zero in the modulated phases.

In order to show that intermediate modulated phases appear in the regions where the transition line has cusps, regions that correspond to the flowers predicted by the mean-field approximation, we have investigated three different ranges of frustration parameters by using anisotropic lattices.

First, we have performed a series of runs for Q/J between 0.13 and 0.17 with a $12\times12\times24$ lattice. In order to observe intermediate phases, the modulation must appear along the largest direction. To prevent the system from choosing the direction at random, we introduce a bias by forcing the modulation of the ground state in the largest direction. We have checked by comparing with cubic simulation cells that the transition temperatures are not changed. This trick guarantees that the transition between different modulations does take place in the largest direction chosen as the z axis. The order parameters is only calculated along this direction, which also saves computer time. For the range of frustration parameters studied, one obtains a sequence of two transitions. Figure 4 shows the variation (with temperature) of two different components of the order parameter, $k_z=\pi/2$ and $k_z=5\pi/12$, for $Q=0.144$. An intermediate phase characterized by a nonzero value of $|M(k_z=5\pi/12)|$, which corresponds to the $\langle 3232^2 \rangle$ mixed lamellar phase, appeared for temperatures between $T\simeq1.85$ and $T\simeq1.77$. At $T\simeq1.85$, the $\langle 3232^2 \rangle$ phase melts into the paramagnetic phase, whereas at $T\simeq1.77$, it transforms to the simple lamellar phase $\langle 2 \rangle$, which is characterized by the ordering wave vector $k_z=\pi/2$ and represents the ground state. The transitions are also observed by monitoring the heat capacity; in Fig. 5, the peak around $T\simeq1.85$ corresponds to the transition between the disordered and the $\langle 3232^2 \rangle$ phase, and the second peak around $T\simeq1.77$ to the transition between this $\langle 3232^2 \rangle$ phase and the $\langle 2 \rangle$ phase. When Q/J increases, the two peaks of the heat capacity versus T curve get closer, and for $Q/J=0.17$, the heat-capacity curve has a single peak [see Fig. 6(a)]. It is

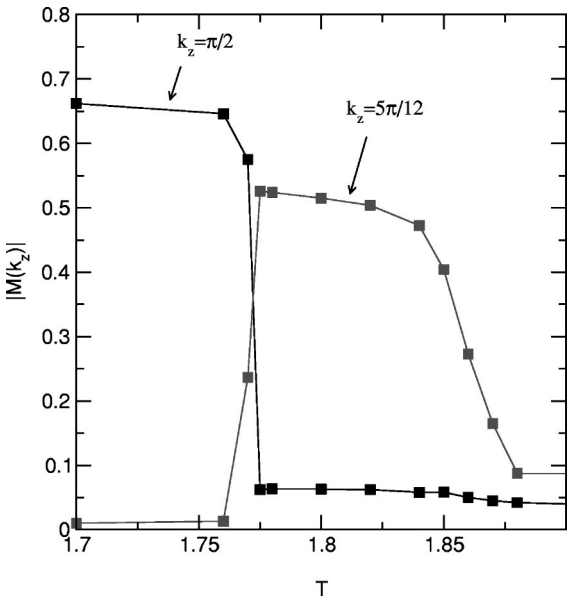

FIG. 4. Order parameter $|M(k_z)|$ vs temperature T for two nonzero ordering wave vectors $k_z=\pi/2$ and $k_z=5\pi/12$ and for $Q/J=0.144$. The first transition appears at $T\simeq1.85$ and corresponds to an ordering wave vector $k_z=5\pi/12$ ($\langle 3232^2 \rangle$ phase); the corresponding order parameter vanishes at a lower temperature $T\simeq1.77$, at which a second transition to a lamellar phase characterized by a nonzero value of $|M(k_z)|$ for $k_z=\pi/2$ ($\langle 2 \rangle$ phase) takes place.

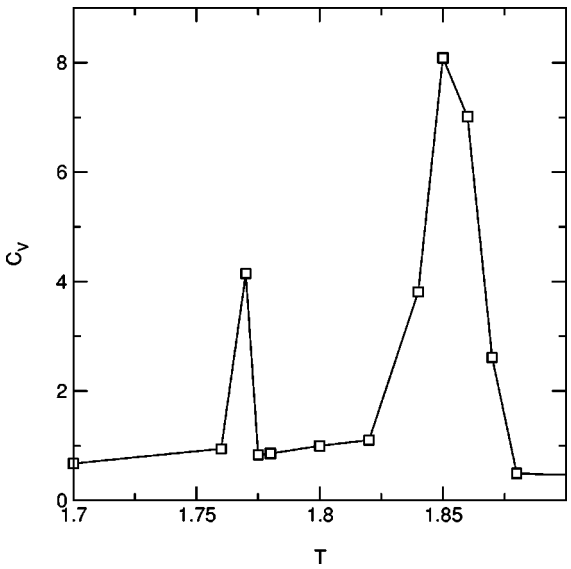

FIG. 5. Specific heat vs temperature for $12\times12\times24$ lattice and for $Q/J=0.144$. The right peak corresponds to the disordered-modulated transition (the modulation is characterized by $k_z=5\pi/12$) and the left peak corresponds to the transition between the $\langle 3232^2 \rangle$ modulated phase (wave vector $k_z=5\pi/12$) and the $\langle 2 \rangle$ phase (wave vector $k_z=\pi/2$).

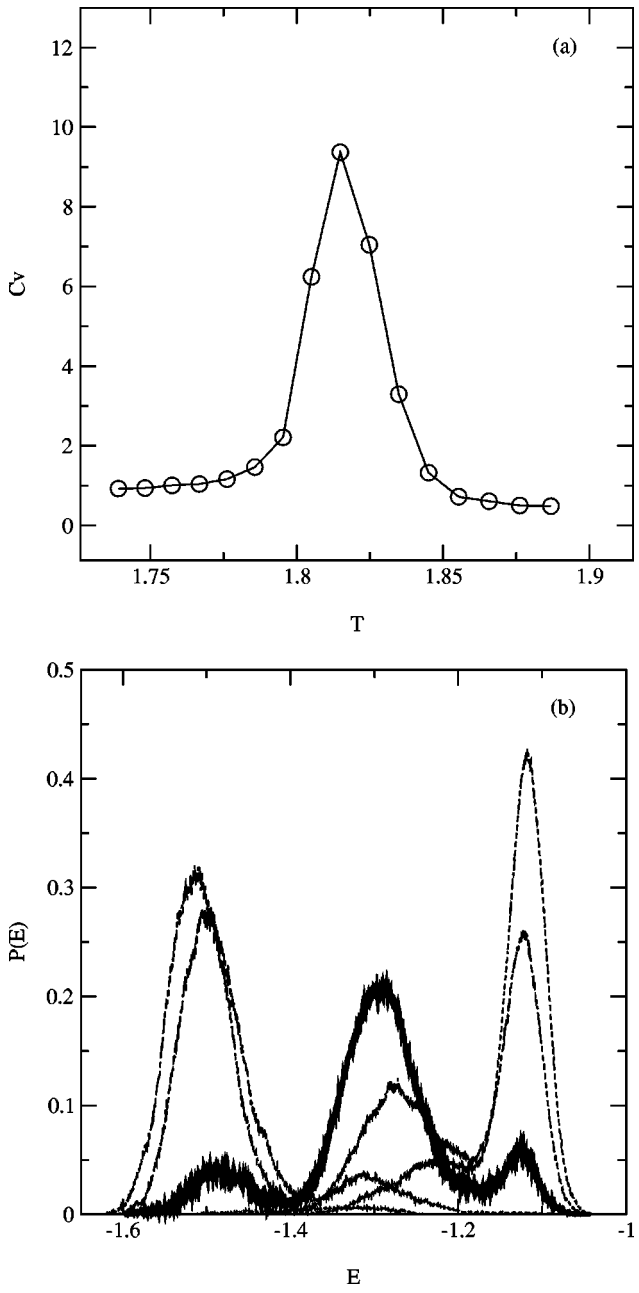

FIG. 6. (a) Specific heat vs temperature for $Q/J=0.17$. (b) Energy histograms for $Q/J=0.17$ at different temperatures $T=1.795$, 1.805, 1.815, 1.825, and 1.835. Note that for $T=1.815$ (thick line) the system is able to flip between three different phases, the paramagnetic, the $\langle 3232^2\rangle$, and the $\langle 2\rangle$ phases and the histogram has three peaks.

worth pointing out that as illustrated in Fig. 6(b), for the temperature corresponding to the peak maximum, the energy histogram has a triple peak structure. The results are summarized on the phase diagram in Fig. 2. We have also considered the region, where Q/J is between 0.12 and 0.127 with a $8\times8\times48$ lattice. One observes an intermediate modulated phase between the paramagnetic phase and the lamellar ground state with an ordering wave vector $k_z=3\pi/8$ (see Fig. 2).

In a second series of simulations, we have focused on

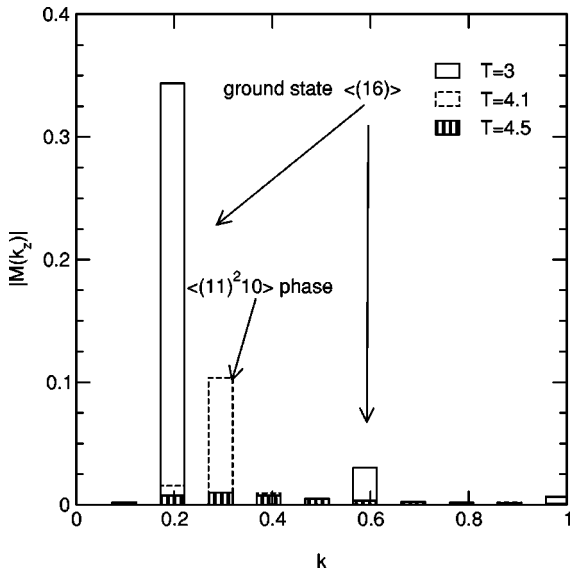

FIG. 7. Order parameter $|M(k_z)|$ vs k_z for $Q/J=0.000\,48$ for three different temperatures. For $T=3$, there are two nonzero components of the order parameter for $k_z=\pi/16$ and $k_z=3\pi/16$, which corresponds to a $\langle(16)\rangle$ simple lamellar phase. For $T=4.1$, the only nonzero component is for $k_z=3\pi/32$, which corresponds to a modulation with a half-period of 64/3 [a $\langle(11)^2 10\rangle$ phase]. For $T=4.5$, all components are zero and the system is paramagnetic.

larger values of Q/J that correspond to the widest flower taking place between the $\langle 1\rangle$ and $\langle 2\rangle$ lamellar phases. The range of frustration parameters, where we have observed intermediate phases, goes from $Q/J=0.55$ to $Q/J=0.90$. We have performed simulations for different lattice sizes, $10\times10\times12$, $10\times10\times14$, and $10\times10\times16$. Intermediate modulated phases occur for these different lattices, but, due to commensurability reasons, the nonzero component of the order parameter is different from one lattice to another. By comparing the energy per site of the three intermediate phases so obtained, we have found that the phase appearing on the $10\times10\times12$ lattice with a nonzero component $k_z=2\pi/3$, is the most stable one for Q/J, between 0.55 and 0.75. This phase is a $\langle 21\rangle$ mixed lamellar phase and is shown in Fig. 2. For $0.75<Q<0.90$, the $10\times10\times12$ lattice has an intermediate phase whose largest nonzero component is for $k_z=5\pi/6$, whereas the $10\times10\times16$ lattice has an intermediate phase whose largest nonzero component is for $k_z=3\pi/4$. This latter phase is more stable and corresponds to a $\langle 21^2\rangle$ mixed lamellar phase (see Fig. 2).

We have also investigated other regions of the phase diagram, where a complex structure of phases is expected. In particular, we have obtained a sequence of two transitions for

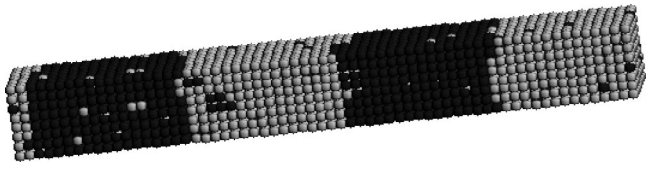

FIG. 8. Spin configuration for a $\langle(16)\rangle$ simple lamellar phase with a half-period of 16 obtained at low temperatures for $Q/J=0.000\,48$ (the lattice is $8\times8\times64$).

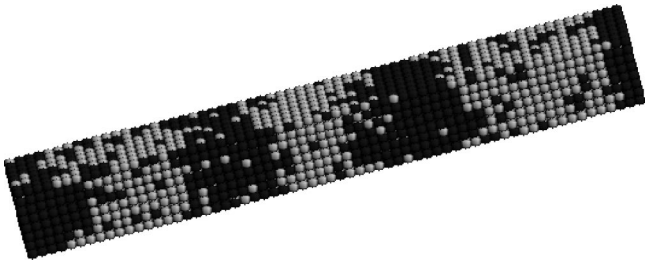

FIG. 9. Spin configuration for a $\langle (11)^2(10) \rangle$ mixed lamellar phase with a half-period of 32/3 obtained at intermediate temperatures for $Q/J=0.000\,48$ (the lattice is $8\times8\times64$).

$Q/J=0.000\,48$. The ground state is a simple $\langle (16) \rangle$ lamellar phase of half-period 16. By using a $8\times8\times64$ lattice, we have observed a transition between the ground state and an $\langle (11)^2(10) \rangle$ mixed lamellar phase of half-period 21.333, ... This is shown in Fig. 7, where the components of the order parameter $|M(k_z)|$ are plotted for $T=3$, 4.1, and 4.5. In the low-temperature region ($T=3$), two components are (significantly) different from zero, namely, $k_z=\pi/16$ and $k_z=3\pi/16$; for $T=4.1$, only one component, $k_z=3\pi/32$ is (significantly) different from zero, and for higher temperatures ($T=4.5$), the system is paramagnetic and the order parameter is identically equal to zero (within the precision of the simulation). Typical spin configurations are displayed in Fig. 8 (ground state) and Fig. 9 (intermediate $\langle (11)^2(10) \rangle$ phase). Table I summarizes the transitions that we have observed for different values of the frustration parameter.

Going further into the details of the (complex) phase diagram would become a very tedious task. The partial phase diagram that we have obtained in the present paper already confirms that the mean-field approach, although incorrect concerning the order of the transition from paramagnetic to modulated phases and overestimating its temperature, provides the right structure for the low-temperature phases. As expected, the mean-field predictions becomes more accurate as lower temperatures are considered (see Figs. 1 and 2).

TABLE I. Observed sequence of transitions for several frustration parameters.

Q/J	Lattice geometry	Phases
0.000 48	$8\times8\times64$	paramagnetic$\rightarrow\langle (11)^2(10) \rangle\rightarrow\langle (16) \rangle$
0.001	$8\times8\times32$	paramagnetic$\rightarrow\langle 65^2 \rangle\rightarrow\langle 8 \rangle$
0.144	$12\times12\times24$	paramagnetic$\rightarrow\langle 3232^2 \rangle\rightarrow\langle 2 \rangle$
0.6	$7\times7\times12$	paramagnetic$\rightarrow\langle 12 \rangle\rightarrow\langle 2 \rangle$

V. CONCLUSION

We have studied the main characteristics of the phase diagram and of the transition for the three-dimensional Coulomb frustrated Ising model by means of refined Monte Carlo algorithms. We have been able to show that the phase diagram retains the complex structure predicted by the mean-field theory. In particular, we have observed in some regions of the temperature-frustration diagram, transitions between different modulated phases corresponding to simple and mixed lamellar patterns. Away from these regions, we have shown by a finite-size scaling analysis, that the melting of modulated phases into the paramagnetic state is a first-order transition, thereby confirming that it is driven from second to first order by the fluctuations.

[1] G. H. Fredrickson and E. Helfand, J. Chem. Phys. **87**, 697 (1987).
[2] H. Fried and K. Binder, J. Chem. Phys. **94**, 8349 (1991).
[3] M. Schulz and K. Binder, J. Chem. Phys. **98**, 655 (1993).
[4] D. Wu, D. Chandler, and B. Smit, J. Phys. Chem. **96**, 4077 (1992).
[5] M. W. Deem and D. Chandler, Phys. Rev. E **49**, 4268 (1994).
[6] H. J. Woo, C. Carraro, and D. Chandler, Phys. Rev. E **52**, 6497 (1995).
[7] T. Garel and S. Doniach, Phys. Rev. B **26**, 325 (1982).
[8] I. Booth, A. B. MacIsaac, J. P. Whitehead, and K. De'Bell, Phys. Rev. Lett. **75**, 950 (1995).
[9] A. B. MacIsaac, J. P. Whitehead, M. C. Robinson, and K. De'Bell, Phys. Rev. B **51**, 16 033 (1995).
[10] V. J. Emery and S. A. Kivelson, Physica C **209**, 597 (1993).
[11] E. W. Carlson, S. A. Kivelson, Z. Nussinov, and V. J. Emery, Phys. Rev. B **57**, 14 704 (1998).
[12] J. Schmalian and P. Wolynes, Phys. Rev. Lett. **85**, 836 (2000).
[13] D. Kivelson, S. A. Kivelson, X. Zhao, Z. Nussinov, and G. Tarjus, Physica A **219**, 27 (1995).
[14] D. Kivelson, G. Tarjus, and S. A. Kivelson, Prog. Theor. Phys. **126**, 289 (1996).
[15] M. Grousson, G. Tarjus, and P. Viot, Phys. Rev. E **62**, 7781 (2000).
[16] S. A. Brazovskii, Sov. Phys. JETP **41**, 85 (1975).
[17] P. Viot and G. Tarjus Europhys. Lett. **44**, 423 (1998).
[18] W. Selke and M. E. Fisher, Phys. Rev. B **20**, 257 (1979).
[19] W. Selke, Phys. Rep. **170**, 213 (1988).
[20] P. Bak and J. von Boehm, Phys. Rev. B **21**, 5297 (1980).
[21] M. H. Jensen and P. Bak, Phys. Rev. B **29**, 6280 (1984).
[22] L. Chayes, V. J. Emery, S. A. Kivelson, Z. Nussinov, and G. Tarjus, Physica A **225**, 129 (1996).
[23] Z. Nussinov, J. Rudnick, S. A. Kivelson, and L. N. Chayes, Phys. Rev. Lett. **83**, 472 (1999).
[24] M. P. Allen and D. J. Tildesley, *Computer Simulation of Liquids* (Clarendon, London, 1987).
[25] K. Binder, Rep. Prog. Phys. **60**, 487 (1997).
[26] R. H. Swendsen and J. S. Wang, Phys. Rev. Lett. **63**, 86 (1989).
[27] U. Wolff, Phys. Rev. Lett. **62**, 361 (1989).
[28] E. Luijten and H. W. J. Blöte, Int. J. Mod. Phys. C **6**, 359 (1995).
[29] E. Luijten and H. W. J. Blöte, Phys. Rev. B **56**, 8945 (1997).
[30] E. Luijten, in *Computer Simulation Studies in Condensed-Matter Physics XII*, edited by D. Landau, S. Lewis, and H.-B. Schüttler (Springer-Verlag, Heidelberg, 2000), p. 86.
[31] C. Dress and W. Krauth, J. Phys. A **28**, L597 (1995).

[32] J. R. Herringa and H. W. J. Blöte, Phys. Rev. E **57**, 4976 (1998).
[33] D. Frenkel and B. Smit, *Understanding Molecular Simulation: From Algorithms to Applications* (Academic, London, 1996).
[34] T. M. MacFarland, G. T. Barkema, and J. F. Marko, Phys. Rev. B **53**, 148 (1996).
[35] K. Hukusima and K. Nemoto, J. Phys. Soc. Jpn. **65**, 1604 (1996).
[36] B. A. Berg and T. Neuhaus, Phys. Rev. Lett. **68**, 9 (1992).